

GSK-3 β -induced Tau pathology drives hippocampal neuronal cell death in Huntington's disease: involvement of astrocyte–neuron interactions

F L'Episcopo^{1,2,8}, J Drouin-Ouellet^{3,8}, C Tirolo¹, A Pulvirenti⁴, R Giugno⁴, N Testa¹, S Caniglia¹, MF Serapide², G Cisbani⁵, RA Barker^{3,6}, F Cicchetti^{5,7} and B Marchetti^{*,1,2}

Glycogen synthase kinase-3 β (GSK-3 β) has emerged as a critical factor in several pathways involved in hippocampal neuronal maintenance and function. In Huntington's disease (HD), there are early hippocampal deficits both in patients and transgenic mouse models, which prompted us to investigate whether disease-specific changes in GSK-3 β expression may underlie these abnormalities. Thirty-three postmortem hippocampal samples from HD patients (neuropathological grades 2–4) and age- and sex-matched normal control cases were analyzed using real-time quantitative reverse transcription PCRs (qPCRs) and immunohistochemistry. *In vitro* and *in vivo* studies looking at hippocampal pathology and GSK-3 β were also undertaken in transgenic R6/2 and wild-type mice. We identified a disease and stage-dependent upregulation of GSK-3 β mRNA and protein levels in the HD hippocampus, with the active isoform pGSK-3 β -Tyr²¹⁶ being strongly expressed in dentate gyrus (DG) neurons and astrocytes at a time when phosphorylation of Tau at the AT8 epitope was also present in these same neurons. This upregulation of pGSK-3 β -Tyr²¹⁶ was also found in the R6/2 hippocampus *in vivo* and linked to the increased vulnerability of primary hippocampal neurons *in vitro*. In addition, the increased expression of GSK-3 β in the astrocytes of R6/2 mice appeared to be the main driver of Tau phosphorylation and caspase3 activation-induced neuronal death, at least in part via an exacerbated production of major proinflammatory mediators. This stage-dependent overactivation of GSK-3 β in HD-affected hippocampal neurons and astrocytes therefore points to GSK-3 β as being a critical factor in the pathological development of this condition. As such, therapeutic targeting of this pathway may help ameliorate neuronal dysfunction in HD.

Cell Death and Disease (2016) 7, e2206; doi:10.1038/cddis.2016.104; published online 28 April 2016

Huntington's disease (HD) is an autosomal-dominant neurodegenerative disorder of the CNS that is characterized by progressive neurological deficits, including involuntary movements (e.g., chorea, dystonia and gait abnormalities), psychiatric disturbances and cognitive decline.¹ Notably, cognitive impairments appear early in the disease course and profoundly impact on the patients' quality of life.^{2,3} This clinical profile reflects the fact that while the major pathology of HD involves the striatum and deep layers of the cerebral cortex,^{1,4–7} it is not restricted to this site but involves many other areas of the CNS from disease onset, including the hippocampus.^{8–10} Both neuronal loss in the hippocampal CA1 region and volumetric reduction on MRI have been reported in patients,^{8–10} which are also seen in animal models of

the disease. All of this suggests that there is a selective vulnerability of hippocampal neurons to the disease process that may explain some of the cognitive and psychiatric deficits commonly seen in HD.¹¹

The genetic basis of HD involves a CAG repeat expansion in exon 1 of the huntingtin (Htt) gene, leading to an abnormally long polyglutamine (polyQ) tract in Htt, a protein widely expressed throughout the brain and peripheral tissues.^{4,12} This mutant form of the huntingtin protein (mHtt) ultimately forms aggregates in a variety of cell types with pathological consequences impacting on a wide range of cellular processes, all of which lead to neuronal dysfunction and eventually cell loss.^{4–7} In astrocytes, the accumulation of mHtt alters several fundamental glial properties that are critical

¹Neuropharmacology Section, OASI Institute for Research and Care on Mental Retardation and Brain Aging, Troina (EN), Italy; ²Department of Biomedical and Biotechnological Sciences (BIOMETEC), Pharmacology and Physiology Sections, University of Catania, Via S. Sofia 64, Catania 95125, Italy; ³Wallenberg Neuroscience Center, Division of Neurobiology and Lund Stem Cell Center, Lund University, BMC A11, Lund S-221 84, Sweden; ⁴Department of Clinical and Experimental Medicine, Mathematics and Computer Science Section, University of Catania, Viale A. Doria, Catania 95125, Italy; ⁵Centre de Recherche du CHU de Québec (CHUQ), Axe Neurosciences, Québec, QC G1V 4G2, Canada; ⁶John van Geest Centre for Brain Repair, Department of Clinical Neuroscience, University of Cambridge, Cambridge CB2 0PY, UK and ⁷Département de Psychiatrie et Neurosciences, Université Laval, Québec, QC G1V 0A6, Canada

*Corresponding author: B Marchetti, Department of Biomedical and Biotechnological Sciences (BIOMETEC), Pharmacology Section, University of Catania, Catania 95125, Italy. Tel: +33 55 722 698; Fax: +39 935 653 327; E-mail: biancamarchetti@libero.it

⁸These authors contributed equally to this work.

Abbreviations: ACM, astrocyte-conditioned media; AR, AR-AO14418; AT8, phospho-PHF-Tau; CV, cresyl violet; DAPI, 4',6-diamino-2-phenylindole; DG, dentate gyrus; DIV, days *in vitro*; FI, fluorescence intensity; GCL, granule cell layer; GFAP, glial fibrillary acidic protein; GSK-3 β , glycogen synthase kinase-3 β ; pGSK-3 β -Tyr²¹⁶, phosphorylated GSK-3 β at Tyrosine 216; HBSS, Hanks' balanced salt solution; HD, Huntington's disease; H₂O₂, hydrogen peroxide; Htt, huntingtin protein; LDH, lactate dehydrogenase; MAP2, microtubule-associated protein 2; MAPT, microtubule-associated protein Tau; mHtt, mutant huntingtin protein; MTT, 3-(4,5-dimethylthiazolyl)-2,5-diphenyltetrazolium bromide; PBS-T, phosphate-buffered saline containing Tween 20; PMI, postmortem interval; polyQ, polyglutamine; qPCR, quantitative PCR; siRNA, small interfering RNA; TG, transgenic; WT, wild type

Received 11.1.16; revised 11.3.16; accepted 15.3.16; Edited by A Verkhratsky

for neuronal survival, and thus this cell may also indirectly contribute to increase neuronal vulnerability and/or neuronal cell death.^{13–18}

Compelling evidence has been recently provided for the existence of Tau-related pathology as a contributing factor to the cognitive deficits seen in patients with HD. Postmortem analysis of HD brains has revealed an increase both in total Tau and its phosphorylated form, as well as its accumulation within mHtt-positive inclusions,¹⁹ including in the hippocampus. Two independent reports followed demonstrating cortical Tau hyperphosphorylation in the R6/2 transgenic (TG) mouse model of HD.^{20,21} Furthermore, we showed that the rate of cognitive decline in a large cohort of HD patients was greater in those possessing the H2 haplotype of the Tau gene (microtubule-associated protein Tau (MAPT)) compared with those with the H1 haplotype.²²

It is thus becoming increasingly clear that HD is a tauopathy at some level,^{19–23} although the molecular pathways involved in this process remain largely obscure. In this respect, it is of interest to note that activation of glycogen synthase kinase-3 β (GSK-3 β) has a role in the phosphorylation of Tau (MAPT), triggering cytoskeleton destabilization, Tau aggregation and neuronal dysfunction/death.^{24–34} Furthermore, upregulation of GSK-3 β also promotes astroglial activation, astrocyte and microglia migration and increased expression of proinflammatory mediators,^{35–37} all of which may impair neuron–glial interactions leading to exacerbation of neuronal vulnerability/loss.^{38,39} As such, this signaling molecule may have a critical role in mediating some of these Tau-related aspects of HD pathology, especially given that several recent studies have reported that GSK-3 β signaling is dysregulated in cellular and rodent models of HD and that GSK-3 inhibitors prevent cellular polyQ toxicity caused by the HD mutation.^{40–45} However, no clear consensus has emerged regarding whether GSK-3 activity is elevated or decreased in different HD-affected brain regions.^{40–47} We thus sought to resolve this by studying one affected brain region in HD, the hippocampus, in both TG mice and human postmortem tissue, especially as very little is known about GSK-3 β transcription as well as the kinase active form of it, phosphorylated GSK-3 beta at Tyrosine 216 (pGSK-3 β -Tyr²¹⁶), which critically mediates neuronal–glial dysfunction/death.^{27,31,33,38,39,48–52}

Results

Tau pathology coincides with neuronal loss in the hippocampus of HD patients. In accordance with recent reports of Tau phosphorylation at the phospho-PHF-Tau (AT8) epitope in the cortex and striatum of human HD brains,²³ we observed the presence of AT8 neuronal inclusions in the granule cell layer (GCL) and hilus of HD hippocampal sections but not of control (CT; Figures 1a–e). Different morphologies of AT8-positive (AT8⁺) cells were observed, including ring-like perinuclear, flame shaped and globular morphologies, together with numerous neuropil threads (Figures 1a–e), reminiscent of that observed in the hippocampus of Alzheimer's disease patients (Figure 1f). These AT8⁺ neuronal inclusions were accompanied by a progressive decrease in the number of cresyl violet-positive

(CV⁺) and microtubule-associated protein-positive (MAP2⁺) neurons in the GCL of HD as compared with CT hippocampal sections (Figures 1g and h), suggesting that pathological Tau expression could contribute to the loss of neurons at this site in HD patients.

Expression levels of GSK-3 β and its kinase active form pGSK-3 β -Tyr²¹⁶ are both increased in the human HD hippocampus. Because GSK-3 β can hyperphosphorylate Tau (pTau) at the majority of its sites, including AT8,^{24–34} we quantified GSK-3 β levels in the HD and CT hippocampal samples (Table 1)⁵³ using quantitative PCR (qPCR). We first analyzed the expression level and stability of 19 candidate reference genes (Supplementary Table S1) by the geNorm,⁵⁴ NormFinder⁵⁵ and BestKeeper programmes,⁵⁶ which ranked RPL13A and RPLP0 as the most stable reference genes (Supplementary Figure S1 and Supplementary Table S2). We next validated the normalization accuracy of RPLP0 using the quantification of glial fibrillary acidic protein (GFAP) gene expression^{1,6,16} and supported expression which showed a significant increase both at the mRNA and protein levels in HD as compared with CT hippocampal samples (Supplementary Figure S3).

Using RPLP0 as a reference gene (Figure 2a), we then found that GSK-3 β mRNA transcripts were significantly increased in the whole HD group ($F = 14.25$; $P = 0.00063$), as well as in the separate HD Grades 2–4 relative to the CT cases, with the Grade 4 group reaching the highest level of significance ($F = 24.385$; $P < 0.001$) as compared with Grade 2 ($F = 5.775$; $P = 0.036$) and Grade 3 ($F = 6.036$; $P = 0.027$) (Figure 2a).

We next investigated whether GSK-3 β overexpression observed in HD hippocampal samples was associated with an increased expression of GSK-3 β at the protein level (Figures 2b–k). In CT hippocampi, GSK-3 β co-localized primarily with MAP2⁺ neurons in the GCL (Figures 2c and d) and in pyramidal cells of Ammon's horn (Figure 2e). MAP2, a neuron-specific phosphoprotein and a substrate for GSK-3 β ,²⁸ was expressed at higher levels within the cell bodies and dendrites in the CT brains, with the GSK-3 β -IR being preferentially distributed in the MAP2⁺ neuronal cytoplasm with little staining in the nucleus (Figures 2c–e). In HD cases, there was a significant increase of GSK-3 β -IR and of double-labeled MAP2⁺/GSK-3 β ⁺ neurons, which was highest in Grade 3 brains ($P < 0.01$, Figure 2b). As observed, a strong GSK-3 β -IR signal was detected in the MAP2⁺ neuronal cytoplasm of GCL neurons (Figures 2f and g) and pyramidal cells of Ammon's horn (Figure 2h). MAP2 expression was markedly reduced within the cell bodies and dendrites of HD (Figures 2g and h) as compared with CT neurons (Figures 2d and e). Double labeling with GFAP and GSK-3 β revealed GSK-3 β expression in a restricted number of astrocytes in CT (Figures 2i and j), whereas its expression was detected in a much greater number of GFAP⁺ astrocytes in HD (Figure 2k), showing a significantly increased ($P < 0.01$) GFAP-IR as well as cell density ($P < 0.01$) in the dentate gyrus (DG) as compared with CT (Supplementary Figures S3B–D).

The regulation of GSK-3 β activity is brought about by complex mechanisms, including phosphorylation.^{29,30,32–34,48–52} Here we focused our analysis on pGSK-3 β -Tyr²¹⁶ as there is substantial evidence that Tyr²¹⁶ phosphorylation of GSK3 β

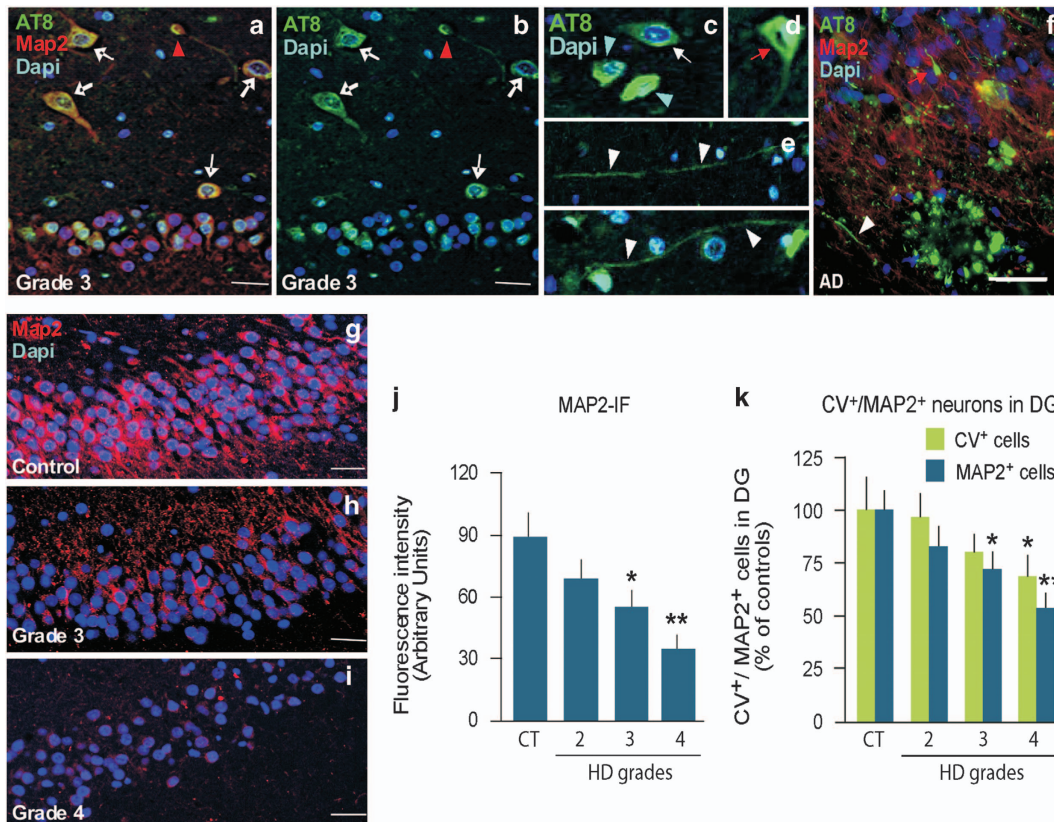


Figure 1 Hyperphosphorylated pathological Tau (AT8) expression coincides with the loss of MAP2-IR in the human HD hippocampus. Hippocampal slide series from HD ($n=5$ cases/severity Grade) and age- and sex-matched CT ($n=6$) were studied. Immunofluorescent staining was carried out on serial paraffin-embedded hippocampal tissue sections ($6\ \mu\text{m}$ in thickness). Cresyl violet staining was used to count the number of neurons present in the GCL. (a–e) Representative images of triple immunofluorescent labeling (a and f) for MAP2⁺ neurons (in red) expressing phosphorylated Tau (AT8, in green) and DAPI (blue). Different morphologies of AT8⁺ cells, including ring-like perinuclear (b, c, white arrow), flame (d, red arrow) and globular inclusions (b, red arrowhead) as well as neuropil threads (e) can be seen in the GCL and hilus of a Grade 3 HD patient and as shown in the DG and hilus of an Alzheimer's disease (AD) patient (f) for comparative purposes. (g–i) MAP2 and DAPI immunofluorescence in a CT (g), Grade 3 (h) and Grade 4 (i) HD case with quantification (j and k) revealing a stage-dependent neuronal decrease in the DG. This result was further confirmed using a quantification of cresyl violet-stained cells against a MAP2 labeling (k). Statistical analysis was performed by one-way analysis of variance with Newman–Keuls Multiple Comparison *posthoc* test. Statistical differences (mean \pm S.D.) in panels (j and k) * $P < 0.05$ versus CT; ** $P < 0.01$ versus CT. Scale bars in panels (a–e), (g–i) = $50\ \mu\text{m}$, (f) = $25\ \mu\text{m}$

represents an important mechanism by which cellular insults can lead to neuronal death^{27,31,33,38,39,48–50} and is known to be stably expressed in the postmortem brains.⁵⁷ We found that, in the CT hippocampus, faint pGSK-3 β -Tyr²¹⁶ labeling could be observed mostly in the cytoplasm of MAP2⁺ neurons (Figures 3c–e) while in HD there was a significant increase ($P < 0.01$; $P < 0.001$) of the active kinase in MAP2⁺ neurons of the DG, with the highest levels detected in Grade 3 HD (Figures 3a, b and f–n). Furthermore, the distribution of pGSK-3 β -Tyr²¹⁶ labeling in MAP2⁺ neurons was different in HD compared with CT, with the pGSK-3 β -Tyr²¹⁶ staining being primarily nuclear (Figures 3h, k and n). This was accompanied by a decrease in the average MAP2 fluorescence intensity (FI) in GCL neurons at the level of the cell bodies and dendrites in the HD samples (Figures 1g, j, 2g, h, 3d, g, j and m). Double staining of pGSK-3 β -Tyr²¹⁶ with astroglial cell markers indicated very little cytoplasmic/nuclear expression of the active kinase in the DG and hilus of the CT hippocampus (Figures 3o, r and s), whereas pGSK-3 β -Tyr²¹⁶-IR signal was detected in greater numbers of HD hippocampal astrocytes (Figures 3p–s). Again, the distribution of pGSK-3 β -Tyr²¹⁶

labeling in HD astrocytes was primarily nuclear (Figures 3p and q). Taken together, these results show that GSK-3 β gene transcription is upregulated in the HD hippocampus and that, at the protein level, GSK-3 β and the active pGSK-3 β -Tyr²¹⁶ isoform are also increased both in neurons and astrocytes in a stage-dependent manner in the HD GCL.

Active pGSK-3 β -Tyr²¹⁶ increases neuronal vulnerability to oxidative stress in R6/2 TG mouse hippocampal neurons. In order to expand on these findings, and given the difficulty of studying causal links in disease pathways in human postmortem tissue, we next turned to the well-characterized R6/2 mouse model of HD.⁵⁸ Using western blotting, we first quantified the levels of active pGSK-3 β -Tyr²¹⁶ in hippocampal tissue from wild-type (WT) and TG mice before (2.5–3 weeks) and after the onset of HD-like features (>8 weeks). We found a 3–4-fold increase of active pGSK-3 β -Tyr²¹⁶ in premanifest and manifest mice (Figures 4a–c) as has recently been reported in the R6/1 mouse model.⁴⁷ In addition, GFAP and AT8 protein levels were significantly increased in R6/2 mice as compared with

WT counterparts (Figures 4a–c). Consistently, astrocytic pGSK-3 β -Tyr²¹⁶-IR was increased in the DG of TG, as compared with that observed in WT mice (Figure 4d). This pGSK-3 β -Tyr²¹⁶ increase was also seen in primary hippocampal neuronal and astrocyte cell cultures derived from R6/2 mice, when compared with active kinase levels detected in WT counterparts (Figure 4e). In agreement with a previous study,²¹ phosphorylation of Tau at the AT8 epitope was not changed in premanifest mice (Figures 4a–c), whereas a significant increase was observed after the onset of the disease when compared with WT mice, suggesting that mHtt can induce Tau hyperphosphorylation with the progression of HD hippocampal pathology.

Accordingly, we next studied the impact of pGSK-3 β -Tyr²¹⁶ on neuronal viability in hippocampal neuronal cultures derived from WT and TG mouse brains. Notably, unlike astrocytes, neurons are highly vulnerable to mHtt *in vitro*^{13–18,40} (Supplementary Figure S4). Consistently, increased pGSK-3 β -Tyr²¹⁶ protein levels (Figures 4f and i) were associated with a reduction in TG neuronal (TG-N) viability, as revealed by decreased mitochondrial activity (Figure 4g), and increased cell death (Figure 4h), as compared with TG astrocytes (TG-A), which showed no change in cell viability as compared with their WT counterparts (Supplementary Figure S4).

Because oxidative stress and mitochondrial dysfunction are critically involved in HD,^{7,59} and given that GSK-3 β becomes activated when apoptotic cell death is initiated,^{27,38,39,48–50} we addressed the contribution of GSK-3 β hyperactivation to the response of TG-N exposed to oxidative stress. A low dose of hydrogen peroxide (H₂O₂) induced only a small increase in pGSK-3 β -Tyr²¹⁶ in WT-N (Figures 4f and i) and a nearly 25% decrease in neuronal viability, as measured using 3-(4,5-dimethylthiazolyl-2)-2,5-diphenyltetrazolium bromide (MTT) reduction and lactate dehydrogenase (LDH) release assays (Figures 4g and h). In contrast, exposure to the same low oxidative challenge in TG neurons further increased the upregulation in GSK-3 β -Tyr²¹⁶ protein levels (Figures 4f and i). This was associated with an additional significant decrease of TG-N (but not TG-A) viability as indicated by the sharp decrease in mitochondrial activity and significant increase in cell death markers (Figures 4g and h, Supplementary Figure S4). Finally, pretreatment with the specific GSK-3 β antagonist AR-AO14418 (*N*-(4-methoxybenzyl)-*N*-(5-nitro-1,3-thiazol-2-yl)urea), AR rescued the TG-N neurons (Figures 4f–i).

TG astrocytes overexpressing pGSK-3 β -Tyr²¹⁶ lose their neurotrophic and neuroprotective properties, exacerbating neuronal loss. Because GSK-3 β upregulation may impair astrocyte–neuron interactions,^{38,39} we next addressed the effects of overexpressing GSK-3 β using different astrocyte–neuron co-culture paradigms and treatments (Figure 5a). In both direct and indirect WT-N/WT-A co-cultures, we confirmed the glial neurotrophic effects, as revealed by increased MAP2 density and neurite length and branching when compared with WT-N cultured without glia (Figures 5b, d, n and o). In striking contrast to WT-A, in the TG-N/TG-A co-culture paradigms, we observed a sharp reduction of MAP2⁺ neurons, associated with reduced neurite length and branching (Figures 5e and o) as compared with WT-N/WT-A counterparts (Figures 5f and o), supporting the concept that mHtt significantly impairs the neurotrophic

Table 1 Characteristics of the human hippocampal samples

ID	Grade	Sex	Age	CAG allele1	CAG allele2
HD1	2	M	73	21	45
HD2	2	M	64	20	45
HD3	2	M	66	19	46
HD4	2	F	78	17	43
HD5	2	M	45	18	47
HD11	3	M	54	23	47
HD12	3	F	61	17	46
HD13	3	M	55	19	51
HD15	3	M	59	19	46
HD16	3	F	65	17	44
HD17	3	M	78	19	43
HD18	3	M	73	21	45
HD21	4	M	44	18	53
HD22	4	M	43	21	53
HD23	4	M	40	18	51
HD24	4	M	47	20	52
HD25	4	M	50	19	50
HD26	4	M	65	18	46
HD27	4	F	26	22	70
HD28	4	M	43	18	51
HD29	4	M	51	20	52
HD30	4	F	53	20	52
HD31	4	M	68	19	45

ID	Sex	Age
CT1	M	75
CT2	M	69
CT3	M	61
CT4	M	67
CT5	M	67
CT6	F	63
CT7	F	61
CT8	M	59
CT9	F	72
CT10	M	67
CT11	M	56
AD1	M	76

properties of astrocytes. Consistently, when TG-A monolayers were placed on top of WT-N, MAP2⁺ neuronal survival was reduced as compared with WT-A/WT-N co-cultures (Figures 5g and o), and conversely, when WT-A were layered on top of TG-N, we observed a significant increase in MAP2⁺ neuronal survival (Figures 5e and o). This implies that mHtt may induce specific astrocyte-derived factors/mechanisms, which are at least in part responsible for reduced neuronal survival. Remarkably, while exposure of WT-N/WT-A cultures to low doses of H₂O₂ was without significant effects on MAP2⁺ cell density (Figures 5j and o), a low oxidative H₂O₂ challenge in TG-N/TG-A co-cultures reduced the numbers of MAP2⁺ neurons (Figures 5l and o), an effect that was even more robust when compared with TG-N cultures alone (Figures 5i, n and o), thereby supporting the contention that, besides other neuronal effects, additional factors linked to the TG-A exacerbate hippocampal TG-N vulnerability.

Depletion of neuronal GSK-3 β attenuates Tau phosphorylation and caspase3 activation in R6/2 neurons. GSK-3 β transgene expression induces Tau hyperphosphorylation with the formation of pretangle structures in the hippocampus, as well as neuronal death, gliosis and learning deficits.²⁵ We thus addressed the specific role of neuronal *versus* astrocyte

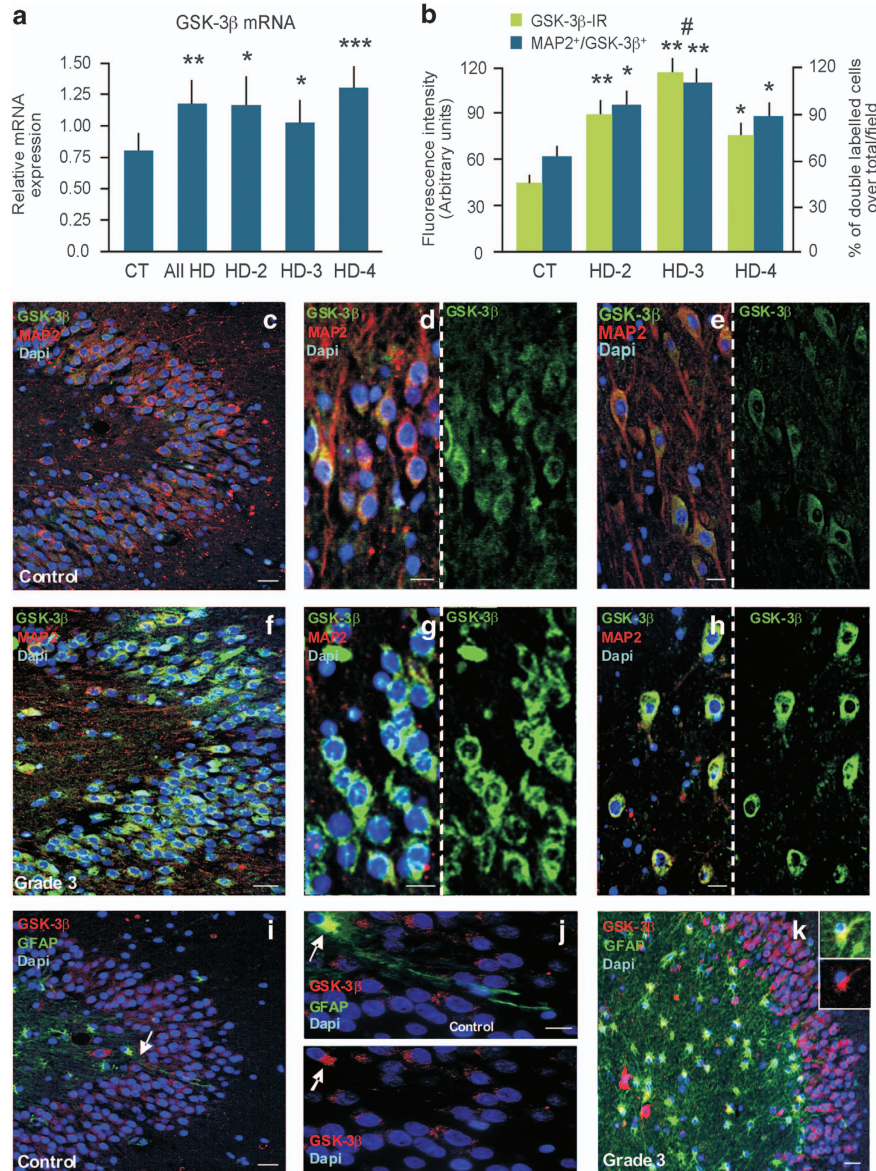


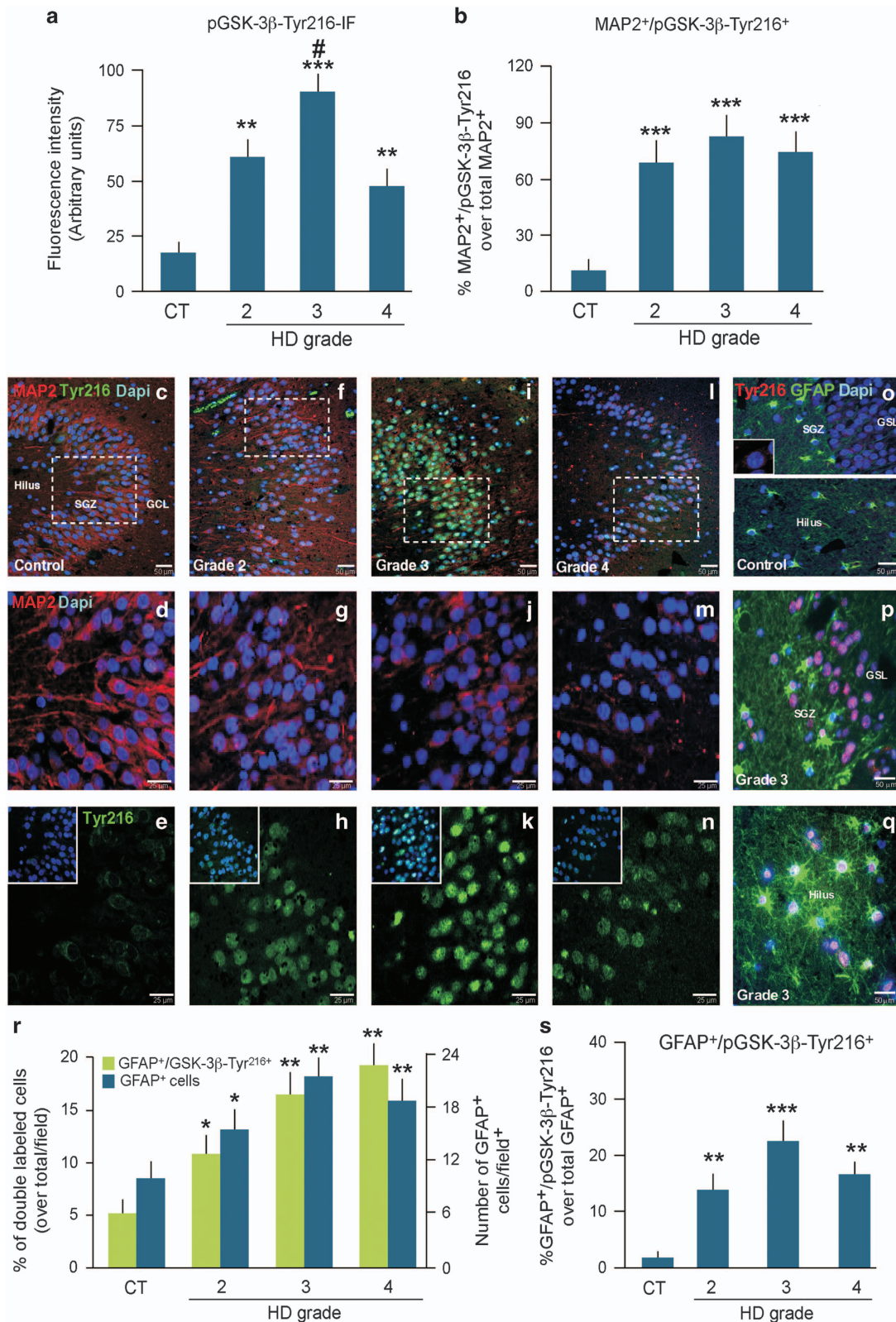
Figure 2 Upregulation of GSK-3 β mRNA and protein levels in GCL neurons and astrocytes in the human HD hippocampus. **(a and b)** qPCR analysis of GSK-3 β transcription and immunoreactivity in CT and HD. The characteristics of the human hippocampal samples are described in Table 1. Statistical analyses were carried out between the total CT and HD groups ($n = 32$) and across grade severity compared with the CT group. Statistical differences in mRNA expression levels (mean \pm S.D.) were determined using a one-way analysis of variance followed by correction for multiple testing using the Tukey's Multiple Comparison test; * $P < 0.05$, ** $P < 0.001$; *** $P = 0.0001$. **(b)** Quantification of GSK-3 β FI and the percentage of MAP2⁺/GSK-3 β ⁺ cells over the total number of MAP2⁺ neurons/field (means \pm S.D.), showing a significant increase of GSK-3 β -IR and of double labeled MAP2⁺/GSK-3 β ⁺ neurons, which was the highest in Grade 3 brains. * $P < 0.05$ and ** $P < 0.01$ versus CT; # $P < 0.05$ versus Grade 4. **(c–h)** Representative images of triple labeling with MAP2 (red), GSK-3 β (green) and DAPI (blue) depicting GSK-3 β expression in the MAP2⁺ neurons in the granular and pyramidal cell layer both in a CT **(c–e)** and a Grade 3 HD brain **(f–h)**. **(i–k)** Triple labeling showing GSK-3 β expression (red) in GFAP⁺ astrocytes (green) and DAPI (blue) in hippocampal sections from CT and HD **(i–k)**. White arrows **(i, j)** show a GSK-3 β (red) expressing GFAP⁺ astrocyte (green) in the GCL of a representative control hippocampal section. Scale bars in panels **(c), (f), (i), (k)** = 50 μ m; **(d), (e), (g), (h), (j)** = 25 μ m

GSK-3 β by investigating the effects of a small interfering (siRNA) against GSK-3 β (siRNA^{GSK-3 β} ^{39,49,60,61}) in either cell type. The introduction of both a CT scrambled siRNA (siRNA^{CT}) or siRNA^{GSK-3 β} was first tested in pilot experiments by qPCR (Figure 6a) and western blotting (Supplementary Figure S5). In WT-N transfected with the siRNA^{CT}, low dose of H₂O₂ induced an approximately 25% decrease in neuronal viability, which was associated with a small increase of caspase3-like activity, whereas GSK-3 β knockdown followed

by H₂O₂ treatment efficiently reversed caspase3 activation-induced cell death (Figures 6b and c). In TG-N transfected with a siRNA^{CT} and treated with PBS, AT8 protein levels were significantly higher when compared with their WT counterpart, whereas in GSK-3 β -depleted TG-N, AT8 protein levels were significantly decreased (Figures 6d and e). These effects were associated with a decrease in DEVD-like fluorescent signal in siRNA^{GSK-3 β} -transfected TG-N, as opposed to TG-N treated with a scrambled siRNA

(Figure 6c), thereby suggesting that TG-N death is associated with mHtt activation of pGSK-3 β /pTau signaling promoting caspase3 activation.

Depleting endogenous GSK-3 β in TG astrocytes reverses Tau phosphorylation and caspase3 activation. Next the effect of GSK-3 β depletion in TG astrocytes was addressed in



the indirect co-culture paradigm. When TG-A were transfected with a siRNA^{CT} and layered on top of TG-N, a sharp loss of MAP2⁺ neurons was observed (Figure 6f), a decrease that was magnified when compared with the decreased MAP2⁺ neurons observed in TG-N alone. When cell death was assessed by caspase3 activation, a greater increase was detected in the TG-A/TG-N indirect co-cultures (Figure 6g) or TG astrocyte-conditioned media (ACM) paradigms (not shown) as compared with the TG-N alone, further supporting astrocyte-induced exacerbation of cell death. Interestingly, these effects were associated with a sharp upregulation of AT8 protein levels (Figures 6h and i) that was significantly greater as compared with TG-N without glia (Figures 6d and e). By contrast, GSK-3 β depletion in TG-glia resulted in a significant reduction of caspase3 activation and AT8 upregulation in TG-N conditioned by TG-A transfected with a siRNA^{CT}, together with a significant enhancement of MAP2⁺ neuronal loss (Figures 6f–m). These findings all suggest that the upregulation of GSK-3 β in TG astrocytes may drive a Tau phosphorylation-induced increase in caspase3, thus exacerbating neuronal death in HD, at least in part, via mHtt-expressing astrocytes.

Finally, we assessed the levels of the proinflammatory cytokines, TNF- α and IL-6, and reactive nitrogen species production and found significantly higher levels in TG-A transfected with a siRNA^{CT} as compared with their WT counterparts (Figure 7a). Especially, H₂O₂ induced additional upregulation of the proinflammatory markers, and this was significantly attenuated by the depletion of GSK-3 β (Figure 7a). Taken together, our findings show that active GSK-3 β is upregulated in the HD hippocampus, both in neurons and astrocytes. This overactivation may potentiate the cytotoxicity of mHtt both directly and indirectly through its influence on astrocytes (Figure 7b).

Discussion

We first analyzed GSK-3 β transcription as a function of disease severity in HD postmortem hippocampal tissue and found that its transcriptional dysregulation is a prominent pathological feature of HD. Extensive immunohistochemistry analyses corroborated our findings by showing increased protein levels for GSK-3 β and active pGSK-3 β -Tyr²¹⁶ in both HD hippocampal neurons and astrocytes as a function of disease severity. Coincident with this pathology, we also found phosphorylation of Tau at the AT8 epitope, as well as a decline in CV⁺/MAP2⁺ neurons in the DG of HD patients.

We then confirmed these findings in a well-recognized (R6/2) HD mouse model, recently shown to develop Tau hyperphosphorylation at multiple Tau phosphoepitopes (AT8, CP13, PT205 and PHF-1) following the onset of HD-like features.²¹ We found an upregulation of both pGSK-3 β -Tyr²¹⁶ and GFAP protein levels in the hippocampus of premanifest R6/2 mice that increased with disease progression. This suggests that mHtt may activate GSK-3 β both at an early stage of the disease process as well as throughout the disease course. Thus we chose to explore this further *in vitro* with experiments, which revealed that there is an upregulation of pGSK-3 β -Tyr²¹⁶ in both primary neurons and astrocytes harvested from the R6/2 mouse brain as well as decreased R6/2 neuronal viability. This, we hypothesized, could be due to an elevated level of oxidative stress. To confirm this, we mimicked such a state by challenging TG-N with a moderate oxidative stimulus and by using a specific GSK-3 β antagonist as well as genetic depletion of GSK-3 β , and we were able to causally link active GSK-3 β to mHtt-induced increased AT8 accumulation, caspase3 activation and R6/2 neuronal cell loss. To further dissect the potential role of R6/2 astrocytes in this process, we used different co-culture paradigms between WT/TG astrocytes and WT/TG neurons. This revealed that TG-A overexpressing GSK-3 β lose their neurotrophic and neuroprotective properties and thus fail to protect and support either WT or TG hippocampal neurons, via, in part, the aberrant production of proinflammatory mediators. Furthermore, depletion of GSK-3 β in R6/2 astrocytes showed that mHtt-induced GSK-3 β overexpression in this cell type is also a crucial factor driving AT8 accumulation, caspase3 activation and reduced neuronal survival. All of this suggests that GSK-3 β overactivation may potentiate mHtt neurotoxic effects both directly and indirectly through an influence on astrocytes (Figure 7b).

Converging evidence implicates GSK-3 β as a key signaling molecule involved in the maintenance and function of adult neurons.^{25–33,38–40,43–45,48–50,59} In particular, GSK-3 β activation has a central role in regulating the neuroinflammatory and astroglial response to neurodegeneration.^{35–39} There is also mounting evidence to show that mHtt impairs astrocyte properties and that this may have an important role in the pathology of HD.^{5,13–18} Taken together, these findings suggest that GSK-3 β dysregulation in both neurons and glia represents a crucial vulnerability factor and a potential target for mitigating the progression of pathology in HD hippocampus.

A special feature of GSK-3 β in neurodegenerative diseases is the phosphorylation of the protein Tau, which is detrimental to neurons. Recently, pathological Tau aggregates have been

Figure 3 Increased expression and translocation of the GSK-3 β -Tyr²¹⁶ isoform in human HD hippocampus. (a) pGSK-3 β -Tyr²¹⁶ immunofluorescence intensity and (b) the number of MAP2⁺ cells expressing pGSK-3 β -Tyr²¹⁶ in HD versus CT ($n = 16$). Statistical differences were determined by a one-way analysis of variance (ANOVA) with Newman-Keuls Multiple Comparison *posthoc* test. ** $P < 0.01$ versus CT; *** $P < 0.001$ versus CT; # $P < 0.05$ versus Grade 4. Note the sharp increase of MAP2⁺ cells expressing pGSK-3 β -Tyr²¹⁶ in Grades 2–4 HD versus CT (b), with the highest level of pGSK-3 β -Tyr²¹⁶-IR being detected in Grade 3 HD (a). (c–n) Representative images depicting triple immunofluorescent labeling of neurons for MAP2 (red), pGSK-3 β -Tyr²¹⁶ (green) and DAPI (blue) in a (c–e) CT, (f–h) Grade 2, (i–k) Grade 3 and (l–n) Grade 4 HD brain. p-GSK-3 β -Tyr²¹⁶ expression in MAP2⁺ neurons have a preferential nuclear distribution in HD cases (f–n), whereas in CT faint immunoreactivity is located within the cytoplasm (c–e). (o–q) Triple immunofluorescent staining of pGSK-3 β -Tyr²¹⁶ (in red), GFAP (in green) and DAPI (blue) revealed scarce cytoplasmic or nuclear expression of the active kinase in the majority of astrocytes in the DG and hilus of CT subjects (o). In HD, both pGSK-3 β -Tyr²¹⁶-negative and pGSK-3 β -Tyr²¹⁶-positive astrocytes were observed in the DG and hilus (p and q). (r and s) The number of astrocytes was greater in the HD hippocampi as compared with CT as well as the level of pGSK-3 β -Tyr²¹⁶ expression. Statistical differences were determined by a one-way ANOVA with Newman-Keuls Multiple Comparison *posthoc* test. * $P < 0.05$ versus CT; ** $P < 0.01$ versus CT; *** $P < 0.001$ versus CT. Changes in the percentage of double-labeled GFAP+/GSK-3 β cells over the total number of GFAP+ cells/field in DG areas (means \pm S.D.) showed that only a limited number of GFAP+ cells expressed GSK-3 β in CT brains, whereas there was a significant increase (** $P < 0.01$ versus CT) of double-labeled astrocytes in HD (o–q). SGZ, subgranular zone

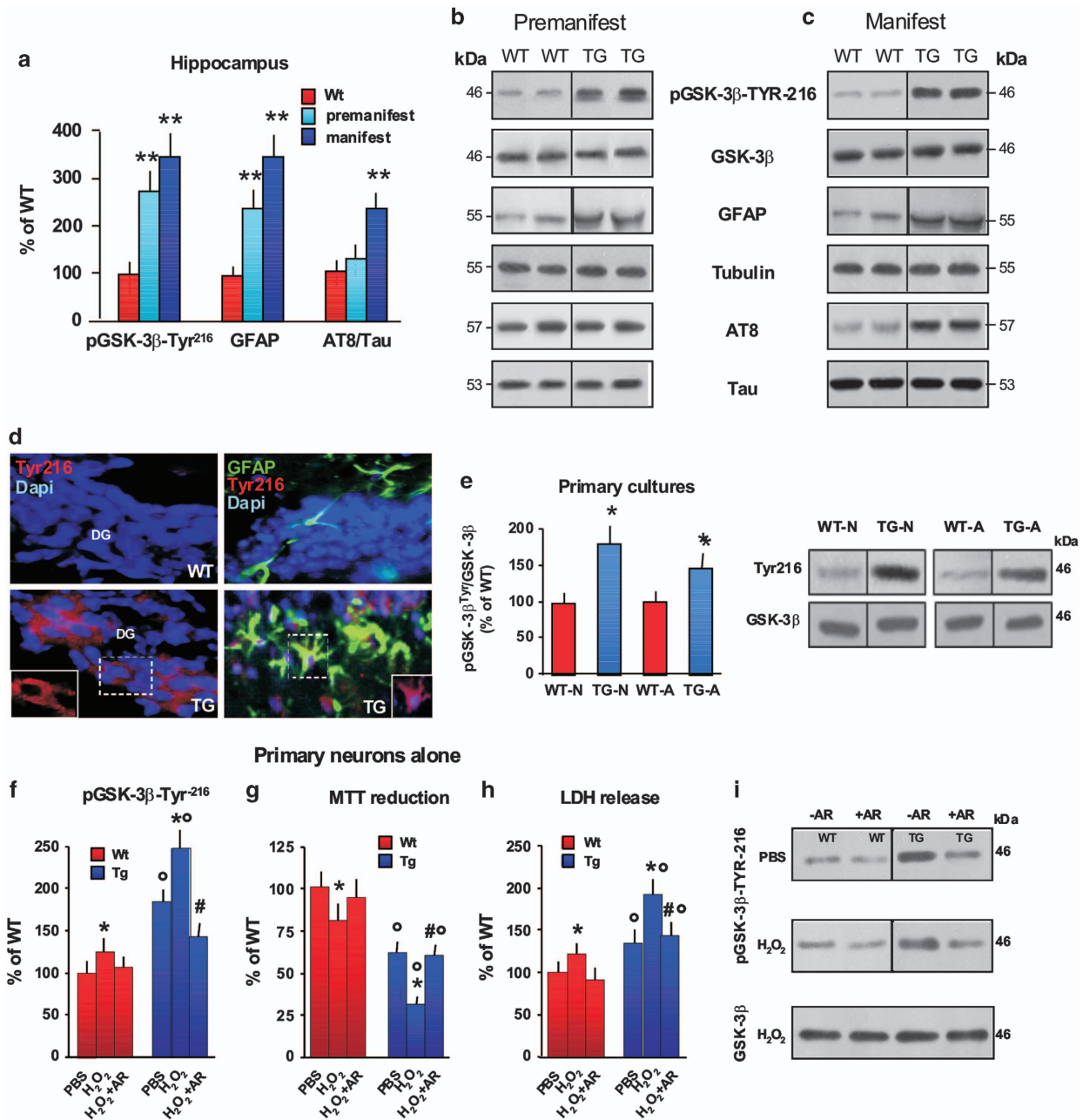


Figure 4 Contribution of active pGSK-3 β -Tyr²¹⁶ to mHtt-induced neuronal death in R6/2 hippocampus. (a–c) Hippocampi were analyzed from WT and TG mice at 3 weeks (premanifest, $n = 6$ each for TG and WT) and ≥ 8 weeks (manifest, $n = 6$ each for TG and WT). Quantification of phosphopeptides was performed versus total GSK-3 β or total Tau, respectively, and normalized to β -tubulin. GFAP quantification was performed versus β -tubulin (as loading control). Results are expressed as the percentage of WT mice. Data are mean \pm S.D. Statistical differences were analyzed by analysis of variance followed by a Newman–Keuls test. $**P < 0.01$ versus WT. (b and c) Two continuous lanes (side by side) from the same blot are displayed for each condition. Black borders correspond to where the images were cropped. (d) Representative immunofluorescent staining of hippocampal sections from 12-week-old WT and R6/2 mice showing increased pGSK-3 β -Tyr²¹⁶-IR in the DG of HD mice, whereas only a faint staining is observed in the WT counterparts. Triple immunofluorescent staining with DAPI (blue), GFAP (green) and pGSK-3 β -Tyr²¹⁶ (red) shows increased staining of the active kinase, which co-localizes with TG but not WT astrocytes. (e) WT and TG mice brains showing increased pGSK-3 β -Tyr²¹⁶ in TG as compared with WT cells and western blotting analysis of pGSK-3 β -Tyr²¹⁶ in primary hippocampal neurons and astrocytes showing increased pGSK-3 β -Tyr²¹⁶ in TG as compared with WT cells. Two representative lanes for neuronal (WT-N, TG-N) and astrocyte (WT-A, TG-A) cells are displayed. $*P < 0.05$ versus WT. (f and i) Western blotting analyses of pGSK-3 β -Tyr²¹⁶ levels in hippocampal neurons at 7–10 DIV after a mild oxidative stress challenge (H_2O_2 , 0.5 μM) in WT and TG cultures, with or without pretreatment (–1 h) with the specific GSK-3 β antagonist AR (5 μM).^{70,73} Two representative continuous lanes are displayed (–AR and +AR) for WT and TG cells, both in PBS- and H_2O_2 -treated conditions. $*P < 0.05$ versus PBS in WT and TG cultures, respectively; $^{\circ}P < 0.01$ versus WT cultures; $^{\#}P < 0.05$ versus H_2O_2 . (g and h): MTT reduction assay and LDH release under basal conditions (PBS) and after a mild oxidative stress challenge (H_2O_2 , 0.5 μM) in WT and TG cultures, in the absence or not of (–1 h) AR (5 μM). Values are expressed relative to untreated WT cells (percentage of WT) and represent the mean \pm S.D. of four replicates. $*P < 0.05$ versus PBS in WT and TG cultures, respectively; $^{\circ}P < 0.01$ versus WT cultures; $^{\#}P < 0.05$ versus H_2O_2 . A, astrocytes; N, neurons

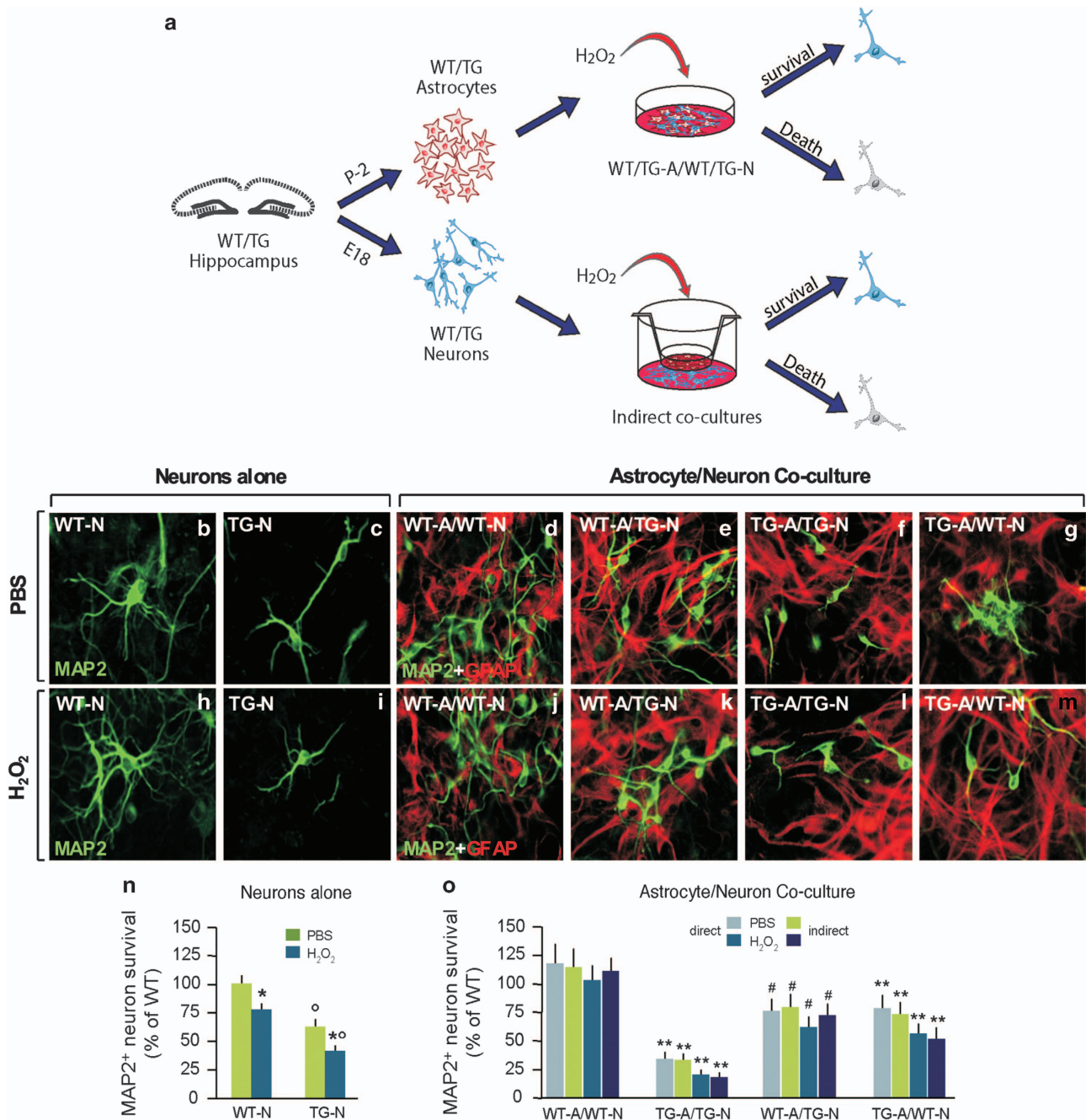


Figure 5 Impaired glial neurotrophic and neuroprotective properties by hyperactive pGSK-3 β -Tyr²¹⁶ in R6/2 astrocytes. **(a)** Schematic drawing showing the co-culture experiments. In the direct co-culture paradigm, WT/TG neurons were layered on top of WT/TG astrocytes for 7–10 DIV, allowing contact between neurons and astrocytes. In the indirect co-culture, glial inserts were added on top of the purified neurons, allowing only factor diffusion. **(b, c, h, i)** Representative images of MAP2+ staining in WT-N and TG-N cultured alone or in the presence (or not) of mild oxidative stress (H₂O₂, 0.5 μ M). **(d–g), (j–m)** Double immunofluorescent staining with GFAP and MAP2 in the direct co-culture paradigms in the absence **(d–g)** or presence **(j–m)** of a mild oxidative stress (H₂O₂, 0.5 μ M). **(n and o)** Neuronal survival as determined by MAP2+ cell counting in the different conditions. Values are expressed as the percentage of WT and represent the mean \pm S.D. of four replicate counts in each condition. Statistical differences were analyzed by analysis of variance followed by a Newman–Keuls test * $P < 0.05$ versus PBS in WT and TG cultures, respectively; ^o $P < 0.01$ versus WT cultures; ** $P < 0.01$ versus WT-A/WT-N; # $P < 0.01$ versus TG-A/TG-N. A, astrocytes; E18, embryonic day 18; N, neurons; P-2, postnatal day 2

seen in cortical and striatal HD tissue,^{22,23} and while our new study did not specifically address this aspect of HD pathogenesis, we did observe AT8 neuronal inclusions in the GCL and hilus of Grades 2–3 hippocampal sections from HD patients. In animal models of HD, Gratzke *et al.*,²¹ have also recently

reported that there is extensive phosphorylation of Tau in the hippocampus, cortex and striatum of R6/2 and 140 CAG knock-in mice, subsequent to the onset of HD pathology,²¹ and the present study corroborates this by showing increased AT8 protein levels in the R6/2 hippocampus. The critical role of

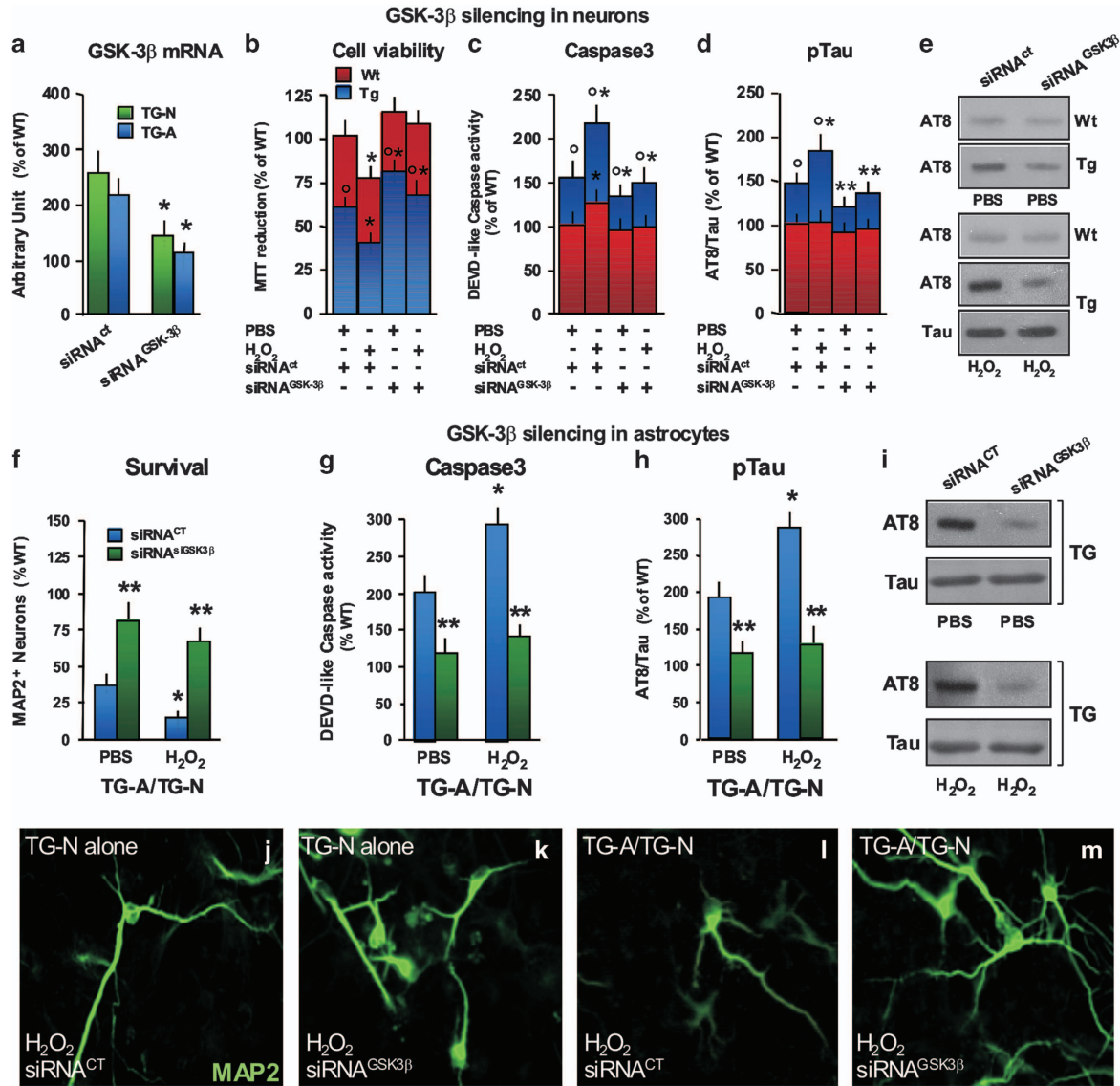


Figure 6 Synergistic effect of neuronal and astrocyte hyperactive GSK-3 β in the exacerbation of Tau phosphorylation and neuronal death in R6/2 hippocampal cultures. (a) qPCR quantification of GSK-3 β mRNA following a treatment with siRNA^{GSK-3 β} or a siRNA^{CT} in neurons. $P < 0.05$ versus siRNA^{CT} within TG-N and TG-A, respectively. (b) Cell viability in the presence of a mild oxidative stress, siRNA^{GSK-3 β} , siRNA^{CT} or PBS was measured with the MTT reduction assay. (c) Caspase3 activity was also measured using the fluorogenic substrate DEVD-AFC. (d and e) Tau phosphorylation at the AT8 epitope was determined by western blotting and quantifications performed against total Tau. Two representative continuous lanes are displayed (siRNA^{CT} and siRNA^{GSK-3 β}) for WT and TG, both in PBS- and H₂O₂-treated conditions. Values are expressed as a percentage of WT cells and represent the mean \pm S.D. of four replicate counts in each condition. Statistical differences were analyzed by analysis of variance followed by a Newman–Keuls test. * $P < 0.05$ versus siRNA^{CT}-PBS-treated cells, within WT and TG cultures, respectively; ° $P < 0.01$ versus WT cultures; * $P < 0.05$ versus siRNA^{CT}-H₂O₂-treated cells. (f–i) Quantification of neuronal survival (f), caspase3 activity (g) as well as Tau phosphorylation at the AT8 epitope (h) following GSK-3 β silencing in TG astrocytes using the indirect co-culture (TG-A/TG-N) paradigm with or without mild oxidative stress. Values are expressed as a percentage of WT cells and represent the mean \pm S.D. of three replicate counts in each condition. * $P < 0.05$ versus PBS-treated cells; ** $P < 0.01$ versus siRNA^{CT} cultures. (j–m) Representative images of MAP2⁺ fluorescent staining of TG-N neurons in the presence of an H₂O₂ challenge when cultured alone (j and k) or with TG-A (l and m).

dysregulated endogenous GSK-3 β in this process was further documented in GSK-3 β -depletion experiments, where GSK-3 β knockdown in TG-N significantly attenuated caspase3 activation and AT8 accumulation. Moreover, we show that there is an additional contribution to this cell loss from changes in GSK-3 β in mHtt-containing astrocytes, supporting astrocyte–neuron interactions as essential components in the neuronal dysfunction that characterises neurodegenerative diseases, including HD.^{5,13–18,38,39,62–65}

This enhanced GSK-3 β activation in TG-A not only impaired their neurotrophic and neuroprotective properties but also significantly contributed to mHtt-induced Tau phosphorylation and caspase3 activation, possibly via an exacerbated production of major proinflammatory mediators (Figure 7), as recently highlighted in the study of Garwood *et al.*⁶⁴ indicating that astrocytes are important for A β -induced Tau phosphorylation, caspase3 activation and cell death.⁶⁴

In conclusion, we have shown that there is mHtt-induced GSK-3 β dysregulation in both neurons and astrocytes of the hippocampus in HD has a crucial role in the evolving pathology seen in this disorder. This may not only explain the selective vulnerability of this structure to the disease process and its clinical expression but also open up new therapeutic avenues by which to slow down or even reverse this currently incurable condition.

Materials and Methods

Study design. The aim of the postmortem work was twofold: (i) to investigate the expression and impact of GSK-3 β and its active pGSK-3 β -Tyr²¹⁶ isoform in the HD hippocampus at different stages of disease; and (ii) to identify reliable endogenous candidate reference genes for normalization of qPCR targeted gene expression in human HD hippocampal tissue. The study was approved by the Ethical Research Committee of the Centre Hospitalier Universitaire de Québec (#A13-02-1138) and the OASI Institute for Research and Care on Mental Retardation and Brain Aging (Troina, EN, Italy) ethical board following the guidelines of the Declaration of Helsinki. Human brain tissues were obtained from the Cambridge Brain Bank and used under full ethical approval (REC 01/177).

Postmortem samples. HD cases (CAG > 35) ranged from 43 to 78 years of age (56.8 \pm 12) years (Table 1). All diagnoses were based on genetic confirmation of the expanded CAG repeat (see Table 1) along with clinical history and histopathological evaluation by an experienced neuropathologist using the Vonsattel classification.⁵³ Sample distribution included Grade 2 ($n=5$), Grade 3 ($n=7$) and Grade 4 ($n=10$) tissues; the mean sizes of the longer and shorter CAG repeats were 48.0 \pm 5.5 and 19.0 \pm 1.4, respectively. The postmortem interval (PMI) was 25.7 \pm 12.4 h and brain acidity–alkalinity (pH) values were 6.54 \pm 0.3. CT samples ($n=11$) were neurologically normal cases, matched for age (65.1 \pm 14 years), PMI (26.4 \pm 9.9 h) and pH values (6.49 \pm 0.38). Fresh frozen dissected hippocampi were used for RNA isolation while paraffin-embedded sections were used for immunofluorescence analyses.

Human reference gene panel. A variety of factors affect reference gene mRNA in postmortem human and rodent brain tissues and a careful and stringent selection of a proper constitutively expressed CT gene prior to qPCR analysis is therefore essential.^{54–56,66} We thus analyzed 19 candidate genes (Human Reference Gene Panel, Roche Applied Bioscience, Penzberg, Germany, <http://www.roche-applied-science.com>) from different abundance and functional classes, derived from literature searches and as presented in Supplementary Table S1.

RNA isolation, cDNA synthesis and qPCR assays. The human hippocampus was dissected (approximately 50 mg) using a cryostat and collected for RNA extraction using an RNeasy Lipid Tissue Mini Kit (Qiagen, Toronto, Ontario, Canada) and RNA extraction procedure carried out as described.⁶⁷ Briefly, hippocampal tissue was homogenized in 1 ml of trizol, followed by the addition of 200 μ l of chloroform. The homogenate was subsequently separated into aqueous and organic phases by centrifugation and ethanol was added to the aqueous phase before being passed through an RNeasy column. RNA was eluted in 30 μ l of RNase-free water. The purity of the RNA was determined by measuring the absorbance A260/A280 in a buffered solution at pH 7.4 using nanodrop. The quality and integrity of the extracted RNA was assayed by agarose gel electrophoresis to detect the presence of ribosomal RNA degradation.⁶⁷ One μ g of RNA was taken for synthesis of complementary DNA (cDNA) using a cDNA Synthesis Kit (Life Technologies Europe BV, Monza, Italy, www.lifetechnologies.com) according to the manufacturer's guidelines. The qPCR was carried out as described^{38,39,60,61} (Supplementary Experimental Procedures), using 50 ng of cDNA and according to the manufacturer's protocol (<http://www.roche-applied-science.com>).

Gene analysis and statistics. To compare gene expression stability and rank, geNorm,⁵⁴ NormFinder⁵⁵ and BestKeeper⁵⁶ algorithms were used as detailed in Supplementary Methods. To maximize power, analyses were applied to three groups: (i) all HD cases combined with the neurologically normal cases (CT) as a single group (A); (ii) the HD group alone (B) and (iii) the CT group alone (C). Non-paired Student's *t*-tests were used to determine whether the CT and HD groups differed on individual reference genes or geomean. To compare the homogeneity of the qPCR values of the 33 samples, we performed a two-sided Grubbs' test

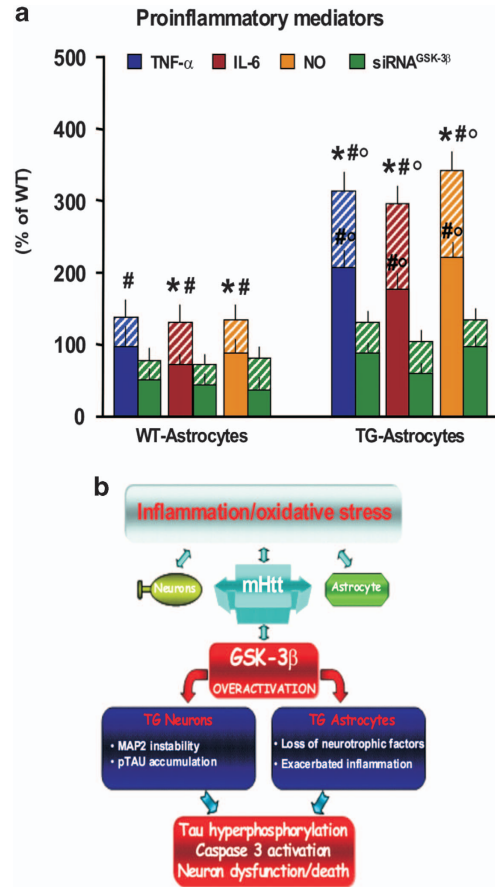


Figure 7 GSK-3 β depletion counteracts cytokine overproduction of R6/2 astrocyte. (a) Astrocytes transfected with either a siRNA^{GSK-3 β} or not with H₂O₂ (0.5 μ M) for 48 h. Levels of TNF- α and IL-6 in the medium were determined using an ELISA.^{68,70} The level of NO in the medium was determined with the Griess reagent.^{68,70} Data are presented as the mean \pm S.E. of three independent experiments. Statistical analysis was performed by one-way analysis of variance with Newman-Keuls Multiple Comparison *posthoc* test; * $P < 0.05$ versus PBS within WT-A and TG-A cultures, # $P < 0.01$ versus WT; $\circ P < 0.01$ versus siRNA^{GSK-3 β} within WT and TG astrocytes, respectively. (b) Astrocytes hyperexpressing GSK-3 β drive Tau phosphorylation and caspase3 activation-induced cell death. Schematic drawing illustrating potential interactions of GSK-3 β in mHtt-induced neuronal toxicity. mHtt-associated GSK-3 β overactivation in hippocampal neurons may increase neuron vulnerability, promoting MAP2 instability and accumulation of pTau. Abnormal activation of GSK-3 β in HD astrocytes may inhibit their neuroprotective functions and progressively exacerbates inflammation.^{34–39,65} All together and in synergy with mHtt-associated neuronal and astrocyte impairments, these effects may further magnify pTau accumulation leading to caspase3-dependent neuronal dysfunction/death

(at significance level $P \leq 0.01$) for each gene. Correlations among continuous variables were performed to determine whether any of the studied variables related to housekeeper/target gene mRNA levels or their geometric means. Statistical significance level was set at $P \leq 0.05$.

Target gene studies. After combinatorial analyses for the selection of a suitable reference gene and validation by comparison with less suitable ones (PPIA, S18) using quantification of the GFAP gene, we addressed changes in mRNA levels of GSK-3 β using RPLP0 as the internal CT gene (Supplementary Figure S3). We used a duplicate assay for each sample. GSK-3 β (ID: Hs01047719-m1), GFAP (ID: Hs00909233-m1), RPLP0 (ID:4326314E), PPIA (ID: 4326316E) and S18 (ID: 4319413E) were obtained from Applied Biosystems (Life Technologies). Quantification of the abundance of target gene expression was determined relative

to the reference gene with respect to the CT group by using the delta delta Ct ($2^{-\Delta\Delta Ct}$) comparative method. Statistical analysis of variance used a one-way ANOVA, followed by correction for multiple testing using the Tukey's Multiple Comparison test.

Immunofluorescence and microscopy analyses. Hippocampal slide series of HD ($n=16$) as well as age- and sex-matched CT ($n=10$) cases were studied. Immunofluorescent staining was carried out on serial paraffin-embedded hippocampal tissue sections ($6\ \mu\text{m}$ in thickness). Adjacent sections were stained with CV acetate (0.1 w/v) to count the number of neurons present in the GCL in each section.^{38,39} Immunostaining was carried out as described previously.^{60,61,67–69} Briefly, after deparaffinization, antigen retrieval was performed by incubating the sections in citrate buffer 10 nM pH 6 at 95 °C for 30 min. The sections were subsequently washed three times in PBS at room temperature (RT). To reduce signal interference from tissue autofluorescence, all sections were incubated with Sudan Black B (Harleco, Philadelphia, PA, USA), 0.5% in 70% alcohol, for 5 min. Sections were washed in PBS containing 0.2% Triton X-100 (3×10 min) between each step. Primary and secondary antibodies (Abs; Supplementary Table S4) were diluted in a blocking buffer of 5% normal serum, 5% bovine serum albumin and 0.4% Triton X-100 in PBS. After overnight incubation with the primary Abs, the sections were rinsed and incubated in darkness for 2 h with CY3/FITC-conjugated donkey anti-rat, donkey anti-rabbit, donkey anti-mouse and donkey anti-goat antibodies (1 : 200–400; Jackson ImmunoResearch, Suffolk, Europe LTD, UK), mounted on glass slides and coverslipped with glycerol-based mounting medium. All Abs used in this study have been previously tested and validated for immunofluorescence and western blotting.^{38,39,60–62,70} Nuclei were counterstained with 4',6-diamino-2-phenylindole (DAPI) in mounting medium, (H1200) Vector Laboratory, Burlingame, CA, USA.

Slides where the primary antibody was omitted served as a negative CT to ensure that there was no autofluorescence from the secondary antibody in the reaction sequence of the labeling experiments. Immunostaining was examined using an Olympus fluorescent microscope BX-51 (Segrate, Milan, Italy) and a Leica TCS-SPE confocal microscope (Leica Lasertechnik GmbH, Heidelberg, Germany).

Confocal laser scanning microscopy, image analysis and quantification of immunostaining. All assessments were performed by a blinded observer. For fluorescent microscopy of hippocampal sections, images were obtained using an inverted Leica LCS-SPE confocal microscope (Leica Lasertechnik GmbH) equipped with an argon/krypton laser or a Fluoroview FV1000 confocal microscope (Olympus Canada Inc., Richmond Hill, Ontario, Canada). For FI assessments and co-localizations, hippocampal sections were labeled by immunofluorescence, and images were acquired by sequential scanning of 12–16 serial optical sections. 3D reconstructions from z-series were used to verify co-localization in the x–y, y–z and x–z planes. To estimate cellular pGSK-3 β -Tyr²¹⁶ fluorescence in the DG, the cell fluorescence was acquired separately with the FITC and CY3 filters, as detailed elsewhere.^{60,69} For cell counting, serial fluorescent images were captured in randomly selected areas along the DG and the number of labeled cells per field (14–18 fields/section) was manually counted in three to four hippocampal sections/case, using the Olympus cellSense Dimension software (Segrate, Milan, Italy), and results expressed as mean \pm S.D.

Studies in R6/2 mice. R6/2 mice, TG for exon 1 of the human Htt gene⁵⁸ and WT littermates were initially obtained from the Jackson Laboratory (Bar Harbor, ME, USA) and mated with female CT mice (B6CBAF1/J). Offspring were verified by a PCR genotyping technique using DNA extracted from tail tissues using primers (5'-CCGCTCAGTTCTGCTTTA-3' and 5'-GGCTGAGGAAGCTGAGGAG-3') located in the transgene. The study was carried out in premanifest (3 weeks of age) and manifest mice (> 8 weeks of age) as the onset of HD features in these mice occurs at 8 weeks of age.⁵⁸ The tail test was used to detect the abnormal clasping of the hind limbs and was employed to ensure the premanifest status of the R6/2 mice.⁵⁸ Mice were suspended by the tail for 10 s; if the mouse acquired a locked body position, the result was scored as positive. The animals were weighed once a week and handled according to National Institutes of Health guidelines. The protocol received approval by the institutional Animal Care and Use Committee, and all studies were conducted in accordance with the United States Public Health Service's Policy on Humane Care and Use of Laboratory Animals.

Primary neuronal cell cultures. Primary cultures of hippocampal neurons were generated from TG R6/2 and WT mice. Briefly, at embryonic day 17, tails from each embryo were used to extract genomic DNA and to perform PCR for genotype determination. The brains were next removed and hippocampi were dissected free of

meninges in Ca²⁺/Mg²⁺-free Hanks' balanced salt solution (HBSS) and rinsed twice with HBSS allowing the tissue to settle to the bottom of the tube. After the second wash, the tissue was resuspended in HBSS containing 0.25% (w/v) trypsin (without phenol red) and incubated for 15 min at 37 °C. After three rinses with HBSS, the tissue was mechanically dissociated in plating medium (Dulbecco's modified Eagle's medium, GIBCO, Rockville, MD, USA), supplemented with 10% horse serum (GIBCO), 100 U/ml penicillin and 100 mg/ml streptomycin by gentle passage through Pasteur pipettes. Dissociated hippocampal cells were seeded in poly-L-lysine-coated six-well culture plates at a density of 7×10^5 cells per well in plating medium. Cultures were maintained at 37 °C in 5% CO₂ for 2 h before the plating medium was replaced with neurobasal growth medium (GIBCO) supplemented with B27 (GIBCO), 2 mM L-glutamine, 100 U/ml penicillin and 100 mg/ml streptomycin. At day 2, cultured neurons were treated with 1- β -D-arabinofuranosylcytosine 2 μM for 24 h.^{38,39} The medium was changed every 3 days, and after 7–10 days in culture (days *in vitro* (DIV)), cells were used for the experiments. The purity of the neuronal cultures ($\geq 95\%$) was determined by immunofluorescence staining for the neuron-specific marker, MAP2.

Primary astrocyte cultures. Primary astrocyte cell cultures were obtained from mouse hippocampi of postnatal 2–3-day-old WT and TG mice, as described previously.^{38,39,60,61,69,71} The cultures were allowed to grow and differentiate until they reached confluency at which time (21–25 DIV) the loosely adherent microglial cells were separated by shaking for 2 h at 37 °C and 190 r.p.m. The attached cells were then washed with sterile PBS and incubated for 1–2 h at 37 °C incubator, at 5% CO₂, before overnight shaking at 37 °C and 210 r.p.m. The supernatant media containing oligodendrocyte precursors and other cell types were discarded. The glial (> 95% of the cells were GFAP-IR astrocytes) monolayers were then rinsed with sterile PBS and replated at a final density of $0.4\text{--}0.6\times 10^5$ cells/cm² in poly-D-lysine (10 $\mu\text{g}/\text{ml}$)-coated 6, 12- or 24-well plates or in insert membranes (0.4 μm polyethylene terephthalate) for indirect co-culture (BD Biosciences, Becton Dickinson Labware, Franklin Lakes, NJ, USA). Astrocyte monolayers were used for direct or indirect co-cultures or processed for gene silencing and used for indirect co-cultures with primary hippocampal neurons, as described. Alternatively, the neuronal cultures were exposed to the ACM.⁶⁹

Preliminary dose–response and time course pilot experiments on neuronal and astrocyte cell viability of WT and TG cultures were first carried out using a range of concentrations of H₂O₂ (0.25–25 μM) and a concentration range of 0.5 μM was selected for the study. Consistent with earlier and more recent reports on primary cortical and striatal R6/2 cultures, we detected an increased vulnerability of hippocampal R6/2 neurons, while the viability of R6/2 astrocytes was not affected by such stressors^{13,17,18,40} (Supplementary Figure S4). Both purified neuronal cultures and astroglial–neuronal co-cultures at 8–9 DIV received PBS or H₂O₂ (0.5 μM). Pharmacological antagonism of GSK-3 β was carried out with the specific GSK-3 β antagonist, AR (of 5 μM)^{38,39,71} administered for 60 min before H₂O₂. Viability assays, caspase3 activity and protein extracts for western blotting determinations of protein levels were carried out as part of these neuronal cultures; other neuronal cultures were used for immunocytochemistry and cell counting. Briefly, the cultures were fixed in 4% paraformaldehyde in PBS and processed using immunofluorescent staining procedures,^{38,39,52,53} employing anti-MAP2 and anti-GFAP, as described above. Nuclei were counterstained with DAPI. Analyses were performed using a confocal laser microscope and computer-assisted image analysis (Leica). For quantification of the amount of cells expressing a given marker or marker combinations, the number of MAP2⁺ cells was determined relative to the total number of DAPI-labeled nuclei, using the Leica lite Software (Leica, Heidelberg, Germany) and three-dimensional overlay to avoid false-positive/negative overlay and double counting.

Cell viability and caspase3 activity assays. Primary neuronal and astrocyte cell cultures treated as above were analyzed for membrane integrity by exclusion of Trypan blue (0.12% wt/vol), metabolic reductase activity using the MTT assay and cell death by the LDH release and caspase3 assay.^{38,39,60,61,69} For the MTT assay, MTT was added to the existing culture medium (final concentration of 120 μM) for 15 min after which the media was removed. Reduced MTT solubilized with 200 μl DMSO was then measured by absorbance at 585 nm. The LDH assay used the LDH Cytotoxicity Detection Kit (Roche) as per the manufacturer's instructions. For caspase3 activity measurements, the cells were lysed in ice-cold lysis buffer and processed as detailed elsewhere.^{38,39,60,61,69} The fluorogenic substrate DEVD-AFC (15 μM ; Calbiochem System Products, San Diego, CA, USA), used for quantification of DEVD-like fluorescent signal, was assessed using a luminescence spectrophotometer (Beckman Coulter, Cassina de' Pecchi, Milan, Italy) (excitation 400 nm and emission 505 nm). Enzymatic activity (arbitrary fluorescent units) is expressed as the percentage of CTs.

Transient gene silencing with siRNA. To test the effect of GSK-3 β protein depletion, we used targeted mRNA degradation using siRNA performed as described previously.^{39,49,60,61} GSK-3 β siRNA (sc-35525) and CT siRNA (sc-37007) were purchased from Santa Cruz Biotechnology (Dallas, TX, USA). siRNA introduction was performed according to the protocol provided by Santa Cruz Biotechnology, as reported in detail in our previous studies.^{39,60,61} Briefly, to prepare lipid–siRNA complexes, 80 pmol of the indicated siRNA duplex in 100 μ l of Transfection medium (sc-36868) and 6 μ l of siRNA Transfection reagent (sc-29528) in 100 μ l of Transfection medium were combined, incubated for 30 min at 25 °C and diluted with 800 μ l of prewarmed Transfection medium. The cells were dissociated and plated on 24 plate cells in growth medium, rinsed once with serum-free DMEM and 1000 μ l of lipid–siRNA mixture (as described above) was applied to each well. After incubation for 6 h at 37 °C in a humidified 5% CO₂ cell culture chamber, an additional 1 ml of 20% FBS in DMEM was added to each well, and lipofection was allowed to continue overnight. The next morning, the lipofection medium was aspirated, and transfected cells were re-fed with fresh growth medium. The cells were collected 72 h after transfection for qPCR and western blotting assays.

Protein extraction and western blotting. For hippocampal tissues, mice were killed by decapitation and the brains immediately removed and the tissues dissected on ice, then frozen on dry ice and kept at –80 °C until studied. Dissected hippocampi were homogenized and processed, as described previously^{38,39} (Supplementary Methods), proteins quantified using the BCA protein determination method (Bio-Rad, Hercules, CA, USA). SDS-PAGE and western blotting analysis of hippocampal samples/cell homogenates were then performed as detailed in L'Episcopo *et al.*⁶¹ and Tunbridge *et al.*⁶⁶ Briefly, hippocampal tissue or cell homogenates were separated on SDS-10% polyacrylamide gel and then transferred onto nitrocellulose membranes (Amersham Biosciences, Pittsburgh, PA, USA). Non-specific binding sites were blocked with 5% non-fat dry milk in phosphate-buffered saline containing 0.1% Tween 20 (PBS-T) for 1 h at RT and were afterwards incubated overnight at 4 °C with the specific antibodies (Supplementary Table S4). The following day, membranes were washed three times in PBS-T and then incubated for 1 h at RT with the corresponding HRP-conjugated secondary antibodies in 5% non-fat dry milk in PBS-T, and the immunoreactive signal intensity was visualized by enhanced chemiluminescence (ECL Plus, GE Healthcare Biosciences, Piscataway, NJ, USA). Immunoreactive bands were visualized using the ImageQuant LAS 4000 imaging system (Fujifilm USA, Valhalla, NY, USA). Quantification of phosphopeptides was performed relative to their non-phosphorylated proteins and was normalized to β -tubulin or β -actin as loading controls. Results are expressed as the percentage of WT mice. Data are mean \pm S.D. with $n=6$ for each condition.

Enzyme-linked immunosorbent assay (ELISA) and NO production. Levels of cytokines were determined using the ELISA kits (DuoSet ELISA Development System, R&D Systems, McKinley Place, MN, USA) following the manufacturer's protocol.^{60,72} NO production was determined by measuring the accumulated levels of nitrite in the culture supernatants with the Griess reagent.^{61,72}

Statistical analyses. Results for immunocytochemistry, immunoblots, *in vitro* viability and caspase3 assays, GSK-3 β depletion experiments and ELISA assays are expressed as mean \pm S.D. unless otherwise noted. Statistical analysis was performed by one-way ANOVA with Newman–Keuls Multiple Comparison *posthoc* test. Statistical significance was accepted at $P<0.05$.

Conflict of Interest

The authors declare no conflict of interest.

Acknowledgements. We thank the Italian Ministry of Health (Ricerca Corrente 2013–2015 to BM), the Italian Ministry of Research and University (MIUR, to BM) and the OASI (IRCCS) Institution Troina (EN) Italy. Part of this research was further funded by a Canadian Institutes of Health Research grant to FC, who is also a recipient of a National Researcher career award from the Fonds de Recherche du Québec en santé (FRQS) providing salary support and operating funds. JDO was supported by a postdoctoral fellowship from FRQS. We also thank the Cambridge Brain Bank for the postmortem tissue that is supported by a grant to the NIHR Cambridge Biomedical Research Centre.

1. Vonsattel JP, DiFiglia M. Huntington's disease. *J Neuropathol Exp Neurol* 1998; **57**: 369–384.
2. Ready RE, Mathews M, Leserman A, Paulsen JS. Patient and caregiver quality of life in Huntington's disease. *Mov Disord* 2008; **23**: 721–726.
3. Novak MJ, Tabrizi SJ. A man with deteriorating ability to live independently. *BMJ* 2011; **24**: 34.
4. DiFiglia M, Sapp E, Chase KO, Davies SW, Bates GP, Vonsattel JP *et al.* Aggregation of huntingtin in neuronal intranuclear inclusions and dystrophic neurites in brain. *Science* 1997; **277**: 1990–1993.
5. Cattaneo E, Rigamonti D, Goffredo D, Zucato C, Squitieri F, Sipione S. Loss of normal huntingtin function: new development in Huntington's disease research. *Trends Neurosci* 2001; **24**: 182–188.
6. Hodges A, Strand AD, Arakagi AK, Kuhn A, Sengstag T, Huhes G *et al.* Regional and cellular gene expression changes in human Huntington's disease brain. *Hum Mol Gen* 2006; **15**: 965–977.
7. Shirendeb U, Reddy AP, Manczak M, Calkins MJ, Mao P, Tagle DA *et al.* Abnormal mitochondrial dynamics, mitochondrial loss and mutant huntingtin oligomers in Huntington's disease: implications for selective neuronal damage. *Hum Mol Gen* 2011; **20**: 1438–1455.
8. Spargo E, Everall PL, Lantos PL. Neuronal loss in the hippocampus in Huntington's disease: a comparison with HIV infection. *J Neurol Neurosurg Psychiatry* 1993; **56**: 487–491.
9. Rosas HD, Koroshetz WJ, Chen YI, Skeuse C, Vangel M, Cudkowicz ME *et al.* Evidence for more widespread cerebral pathology in early HD: an MRI-based morphometric analysis. *Neurology* 2003; **60**: 1615–1620.
10. Ransome MJ, Renoir T, Hannan AJ. Hippocampal neurogenesis, cognitive deficits and affective disorder in Huntington's disease. *Neural Plast* 2012; **2012**: 874387.
11. Begefi F, Schwab LC, Mason SL, Barker RA. Hippocampal dysfunction defines disease onset in Huntington's disease. *J Neurol Neurosurg Psychiatry* 2016 (e-pub ahead of print; doi:10.1136/jnnp-2015-312413).
12. The Huntington's Disease Collaborative Research Group. A novel gene containing a trinucleotide repeat that is expanded and unstable on Huntington's disease chromosomes. *Cell* 1993; **72**: 971–983.
13. Shin JY, Fang ZH, Yu ZX, Wang CE, Li SH, Li XJ. Expression of mutant huntingtin in glial cells contributes to neuronal excitotoxicity. *J Cell Biol* 2005; **171**: 1001–1012.
14. Bradford J, Shin JY, Roberts M, Wang CE, Li XJ, Li S. Expression of mutant huntingtin in mouse brain astrocytes causes age-dependent neurological symptoms. *Proc Natl Acad Sci USA* 2009; **106**: 22480–22485.
15. Bradford J, Shin JY, Roberts M, Wang CE, Sheng G, Li S *et al.* Mutant huntingtin in glial cells exacerbates neurological symptoms of Huntington's disease mice. *J Biol Chem* 2010; **285**: 10653–10661.
16. Faideau M, Kim J, Cormier K, Gilmore R, Welch M, Auregan G *et al.* In vivo expression of polyglutamine-expanded huntingtin by mouse striatal astrocytes impairs glutamate transport: a correlation with Huntington's disease subjects. *Hum Mol Gen* 2010; **15**: 3053–3067.
17. Hsiao HJ, Chen YC, Chen HM, Tu PH, Cern Y. A critical role of astrocyte-mediated nuclear factor- κ B-dependent inflammation in Huntington's disease. *Hum Mol Gen* 2013; **22**: 1826–1843.
18. Valenza M, Marullo M, Di Paolo E, Cesana E, Zuccato C, Biella G *et al.* Disruption of astrocyte–neuron cholesterol crosstalk affects neuronal function in Huntington's disease. *Cell Death Differ* 2015; **22**: 690–702.
19. Fernandez-Nogales M, Cabrera JR, Santos-Galindo M, Hoozemans JJ, Ferrer I, Rozemuller AJ *et al.* Huntington's disease is a four-repeat tauopathy with tau nuclear rods. *Nat Med* 2014; **8**: 881–885.
20. Blum D, Herrera F, Francelle L, Mendes T, Basquin M, Obriot H *et al.* Mutant huntingtin alters Tau phosphorylation and subcellular distribution. *Hum Mol Gen* 2015; **24**: 76–85.
21. Gratzue M, Noël A, Julien C, Cisbani G, Milot-Rousseau P, Morin F *et al.* Tau hyperphosphorylation and deregulation of calcineurin in mouse models of Huntington's disease. *Hum Mol Gen* 2015; **24**: 86–99.
22. Vuono R, Winder-Rhodes S, de Silva R, Cisbani G, Drouin-Ouellet J, REGISTRY Investigators of the European Huntington's Disease Network, *et al.* The role of tau in the pathological process and clinical expression of Huntington's disease. *Brain* 2015; **138**: 1907–1918.
23. Gratzue M, Cisbani G, Cicchetti F, Planel E. Is Huntington's disease a tauopathy? *Brain* 2016; **139**: 1014–1025.
24. Hanger DP, Hughes K, Woodgett JR, Brion JP, Anderton BH. Glycogen synthase kinase-3 induces Alzheimer's disease-like phosphorylation of tau: generation of paired helical filament epitopes and neuronal localisation of the kinase. *Neurosci Lett* 1992; **147**: 58–62.
25. Lucas JJ, Hernandez F, Gomez-Ramos P, Moran MA, Hen R, Avila J. Decreased nuclear β -catenin, tau hyperphosphorylation and neurodegeneration in GSK-3 β conditional transgenic mouse. *EMBO J* 2001; **20**: 27–39.
26. Leroy K, Yilmaz Z, Brion JP. Increased level of active GSK-3 β in Alzheimer's disease and accumulation in argyrophilic grains and in neurones at different stages of neurofibrillary degeneration. *Neuropathol Appl Neurobiol* 2007; **33**: 43–55.
27. Duka T, Duka V, Joyce JN, Sidhu A. α -Synuclein contributes to GSK-3 β catalyzed Tau phosphorylation in Parkinson's disease models. *FASEB J* 2009; **23**: 2820–2830.
28. Sierrol-Piquier M, Gomez-Ramos P, Hernandez F, Perez M, Morán MA, Fuster-Matanzo A *et al.* GSK3 β overexpression induces neuronal death and a depletion of the neurogenic niches in the dentate gyrus. *Hippocampus* 2011; **21**: 910–922.
29. Medina M, Wandosell F. Deconstructing GSK-3: the fine regulation of its activity. *Int J Alzheimers Dis* 2011; **2011**: 479249.
30. Kaidanovich-Beilin O, Woodgett JR. GSK-3: functional insights from cell biology and animal models. *Front Mol Neurosci* 2011; **4**: 40.

31. Duka V, Lee JH, Credle J, Wills J, Oaks A, Smolinsky C *et al*. Identification of the sites of tau hyperphosphorylation and activation of tau kinases in synucleinopathies and Alzheimer's diseases. *PLoS One* 2013; **8**: e75025.
32. Llorens-Martin ML, Jurado J, Hernández F, Ávila J. GSK-3 β , a pivotal kinase in Alzheimer disease. *Front Mol Neurosci* 2014; **21**: 7–46.
33. Credle JJ, George JL, Wills J, Duka V, Shah K, Lee YC *et al*. GSK-3 β dysregulation contributes to parkinson's-like pathophysiology with associated region-specific phosphorylation and accumulation of tau and α -synuclein. *Cell Death Differ* 2015; **22**: 838–851.
34. Beurel E, Grieco SF, Jope RS. Glycogen synthase kinase 3 beta (GSK3): Regulation, actions and diseases. *Pharmacol Ther* 2015; **148**: 114–131.
35. Beurel E, Jope RS. Lypopolysaccharide-induced interleukin-6 production is controlled by glycogen synthase kinase-3 and STAT3 in the brain. *J Neuroinflammation* 2009; **6**: 9–19.
36. Beurel E, Michalek SM, Jope RS. Innate and adaptive immune responses regulated by glycogen synthase kinase-3 (GSK3). *Trends Immunol* 2010; **31**: 24–31.
37. Wang HM, Zhang T, Li Q, Huang JK, Chen RF, Sun XJ. Inhibition of glycogen synthase kinase-3 β by lithium chloride suppresses 6-hydroxydopamine-induced inflammatory response in primary cultured astrocytes. *Neurochem Int* 2013; **63**: 345–353.
38. L'Episcopo F, Tirolo C, Testa N, Caniglia S, Morale MC, Cossetti C *et al*. Reactive astrocytes and Wnt/ β -catenin signaling link nigrostriatal injury to repair in 1-methyl-4-phenyl-1,2,3,6-tetrahydropyridine model of Parkinson's disease. *Neurobiol Dis* 2011; **41**: 508–527.
39. L'Episcopo F, Serapide MF, Tirolo C, Testa N, Caniglia S, Morale MC *et al*. A Wnt1 regulated Frizzled-1/ β -catenin signaling pathway as a candidate regulatory circuit controlling mesencephalic dopaminergic neuron-astrocyte crosstalk: the therapeutic relevance for neuron survival and neuroprotection. *Mol Neurodegen* 2011; **13**: 6–49.
40. Valencia A, Reeves PB, Sapp E, Li X, Alexander J, Kegel KB *et al*. Mutant huntingtin and glycogen synthase kinase 3-beta accumulate in neuronal lipid rafts of a presymptomatic knock-in mouse model of Huntington's disease. *J Neurosci Res* 2010; **88**: 179–190.
41. van Eyk CL, O'Keefe LV, Lawlor KT, Samaraweera SE, McLeod CJ, Price GR *et al*. Perturbation of the Akt/Gsk3- β signalling pathway is common to Drosophila expressing expanded untranslated CAG, CUG and AUUCU repeat RNAs. *Hum Mol Gen* 2011; **20**: 783–794.
42. Lejeune FX, Mesrob L, Parmentier F, Bicep C, Vazquez-Manrique RP, Parker JA *et al*. Large-scale functional RNAi screen in *C. elegans* identifies genes that regulate the dysfunction of mutant polyglutamine neurons. *BMC Genomics* 2012; **13**: 91.
43. Carmichael J, Sugars KL, Bao YP, Rubinsztein DC. Glycogen synthase kinase-3beta inhibitors prevent cellular polyglutamine toxicity caused by the Huntington's disease mutation. *J Biol Chem* 2002; **277**: 33791–33798.
44. Berger Z, Tlofi EK, Michel CH, Pasco MY, Tenant S, Rubinsztein DC *et al*. Lithium rescues toxicity of aggregate-prone proteins in Drosophila by perturbing Wnt pathway. *Hum Mol Gen* 2005; **14**: 3003–3011.
45. Scheuing L, Chiu CT, Liao HM, Linares GR, Chuang DM. Preclinical and clinical investigations of mood stabilizers for Huntington's disease: what have we learned? *Int J Biol Sci* 2014; **10**: 1024–1038.
46. Lim NK, Hung LW, Pang TY, Mclean CA, Liddell JR, Hilton JB *et al*. Localized changes to glycogen synthase kinase-3 and collapsin response mediator protein-2 in the Huntington's disease affected brain. *Hum Mol Gen* 2014; **23**: 4051–4063.
47. Fernández-Nogales M, Hernández F, Miguez A, Alberch J, Ginés S, Pérez-Navarro E *et al*. Decreased glycogen synthase kinase-3 levels and activity contribute to Huntington's disease. *Hum Mol Gen* 2015; **24**: 5040–5042.
48. Chen G, Bower KA, Ma C, Fang S, Thiele CJ, Luo J. Glycogen synthase kinase 3 β (GSK3 β) mediates 6-hydroxy dopamine-induced neuronal death. *FASEB J* 2004; **18**: 1162–1164.
49. Petit-Paitel A, Brau F, Cazareth J, Chabry J. Involvement of cytosolic and mitochondrial GSK-3beta in mitochondrial dysfunction and neuronal cell death of MPTP/MPP+ treated neurons. *PLoS One* 2009; **4**: e5491.
50. Hongo H, Kihara T, Kume T, Izumi Y, Niidome T, Sugimoto H *et al*. Glycogen synthase kinase-3 β activation mediates rotenone-induced cytotoxicity with the involvement of microtubule destabilization. *Biochem Biophys Res Commun* 2012; **426**: 94–99.
51. Cole A, Frame S, Cohen P. Further evidence that the tyrosine phosphorylation of glycogen synthase kinase-3 (GSK3) in mammalian cells is an autophosphorylation event. *Biochem J* 2004; **377**: 249–255.
52. Lochhead PA, Kinstrie R, Sibbet G, Rawjee T, Morrice N, Cleghon V. A chaperone-dependent GSK3beta transitional intermediate mediates activation loop autophosphorylation. *Mol Cell* 2006; **24**: 627–633.
53. Vonsattel JP, Myers RH, Stevens TJ, Ferrante RJ, Bird ED, Richardson EP Jr. Neuropathological classification of Huntington's disease. *J Neuropathol Exp Neurol* 1985; **44**: 559–577.
54. Vandesompele J, De Preter K, Pattyn F, Poppe B, Van Roy N, De Paepe A *et al*. Accurate normalization of real-time quantitative RT-PCR data by geometric averaging of multiple internal control genes. *Genome Biol* 2002; **3**: RESEARCH0034.
55. Andersen C, Jensen JL, Orntoft TF. Normalization of real-time quantitative reverse transcription-PCR data: a model-based variance estimation approach to identify genes suited for normalization, applied to bladder and colon cancer data sets. *Cancer Res* 2004; **64**: 5245–5250.
56. Pfaffl MW, Horgan GW, Dempfle L. Relative expression software tool (REST) for group-wise comparison and statistical analysis of relative expression results in real-time PCR. *Nucleic Acid Res* 2002; **30**: e36.
57. Li X, Friedman AB, Ro MS, Jope RS. Anesthesia and post-mortem interval profoundly influences the regulatory serine phosphorylation of glycogen synthase kinase-3 in mouse brain. *J Neurochem* 2005; **92**: 701–704.
58. Mangiarini L, Sathasivam K, Seller M, Cozens B, Harper A, Hetherington C *et al*. Exon 1 of the HD gene with an expanded CAG repeat is sufficient to cause a progressive neurological phenotype in transgenic mice. *Cell* 1996; **87**: 493–506.
59. Valencia A, Sapp E, Reeves PB, Alexander J, Masso N, Li X *et al*. Reagents that block neuronal death from Huntington's disease also curb oxidative stress. *Neuroreport* 2012; **23**: 10–15.
60. L'Episcopo F, Tirolo C, Testa N, Caniglia S, Morale MC, Impagnatiello F *et al*. Aging-induced Nrf2-ARE pathway disruption in the subventricular zone drives neurogenic impairment in parkinsonian mice via PI3K-Wnt/ β -catenin dysregulation. *J Neurosci* 2013; **33**: 1462–1485.
61. L'Episcopo F, Tirolo C, Testa N, Caniglia S, Morale MC, Deleidi M *et al*. Plasticity of subventricular zone neuroprogenitors in MPTP (1-methyl-4-phenyl-1,2,3,6-tetrahydropyridine) mouse model of Parkinson's disease involves crosstalk between inflammatory and Wnt/ β -catenin signaling pathways: functional consequences for neuroprotection and repair. *J Neurosci* 2012; **32**: 2062–2085.
62. L'Episcopo F, Tirolo C, Testa N, Caniglia S, Morale MC, Marchetti B. Glia as a turning point in the therapeutic strategy of Parkinson's disease. *CNS Neurol Disord* 2010; **9**: 349–372.
63. Marchetti B, L'Episcopo F, Morale MC, Tirolo C, Testa N, Caniglia S *et al*. Uncovering novel actors in astrocyte-neuron crosstalk in Parkinson's disease: The Wnt/ β -catenin signaling cascade as the common final pathway for neuroprotection and self-repair. *Eur J Neurosci* 2013; **37**: 1550–1563.
64. Garwood CJ, Pooler AM, Atherton J, Hanger DP, Noble W. Astrocytes are important mediators of A β -induced neurotoxicity and tau phosphorylation in primary culture. *Cell Death Dis* 2011; **2**: e167.
65. Marchetti B, Pluchino S. Wnt your brain be inflamed? Yes, it Wnt! *Trends Mol Med* 2013; **19**: 144–156.
66. Tunbridge EM, Eastwood SL, Harrison PJ. Changed relative to what? Housekeeping genes and normalization strategies in human brain gene expression studies. *Biol Psychiatry* 2011; **69**: 173–179.
67. Drouin-Ouellet J, Sawiak SJ, Cisbani G, Lagacé M, Kuan WL, Saint-Pierre M *et al*. Cerebrovascular and blood-brain barrier impairments in Huntington's disease: potential implications for the pathophysiology. *Ann Neurol* 2015; **78**: 160–177.
68. Cicchetti F, Lacroix S, Cisbani G, Vallières N, Saint-Pierre M, St-Amour I *et al*. Mutant huntingtin is present in neuronal grafts in Huntington disease patients. *Ann Neurol* 2014; **76**: 31–42.
69. Gennuso F, Ferneti C, Tirolo C, Testa N, L'Episcopo F, Caniglia S *et al*. Bilirubin protects astrocytes from its own toxicity inducing up-regulation and translocation of multigrin resistance-associated protein 1 (Mrp 1). *Proc Natl Acad Sci USA* 2004; **101**: 2470–2475.
70. Senatorov VV, Ren M, Kanai H, Wei H, Chuang DM. Short-term lithium treatment promotes neuronal survival and proliferation in rat striatum infused with quinolinic acid, an excitotoxic model of Huntington's disease. *Mol Psychiatry* 2004; **9**: 371–385.
71. Gallo F, Morale MC, Spina-Purrello V, Tirolo C, Testa N, Farinella Z *et al*. Basic fibroblast growth factor (bFGF) acts on both neurons and glia to mediate the neurotrophic effects of astrocytes on LHRH neurons in culture. *Synapse* 2000; **36**: 233–253.
72. L'Episcopo F, Tirolo C, Testa N, Caniglia S, Morale MC, Impagnatiello F *et al*. Switching the microglial harmful phenotype promotes lifelong restoration of substantia nigra dopaminergic neurons from inflammatory neurodegeneration in aged mice. *Rejuvenation Res* 2011; **14**: 411–424.
73. Bhat R, Xue Y, Berg S, Helberg S, Ormo M, Nilsson Y *et al*. Structural insight and biological effect of glycogen synthase kinase 3-specific inhibitor AR-A014418. *J Biol Chem* 2003; **278**: 45937–45945.



Cell Death and Disease is an open-access journal published by Nature Publishing Group. This work is licensed under a Creative Commons Attribution 4.0 International License. The images or other third party material in this article are included in the article's Creative Commons license, unless indicated otherwise in the credit line; if the material is not included under the Creative Commons license, users will need to obtain permission from the license holder to reproduce the material. To view a copy of this license, visit <http://creativecommons.org/licenses/by/4.0/>

Supplementary Information accompanies this paper on Cell Death and Disease website (<http://www.nature.com/cddis>)